pH-Responsive Peptide Mimic Shell Cross-Linked Magnetic Nanocarriers for Combination Therapy

*Kanhu C. Barick, Sarika Singh, Neena V. Jadhav, Dhirendra Bahadur, Badri N. Pandey, and Puthusserickal A. Hassan**

The design and development of water dispersible, pH responsive peptide mimic shell cross-linked magnetic nanocarriers (PMNCs) using a facile soft-chemical approach is reported. These nanocarriers have an average size about 10 nm, are resistant to protein adsorption in physiological medium, and transform from a negatively charged to a positively charged form in the acidic environment. The terminal amino acid on the shell of the magnetic nanocarriers allows us to create functionalized exteriors with high densities of organic moieties (both amine and carboxyl) for conjugation of drug molecules. The drug-loading efficiency of the nanocarriers is investigated using doxorubicin hydrochloride (DOX) as a model drug to evaluate their potential as a carrier system. Results show high loading affinity of nanocarriers for anticancer drug, their sustained release profile, magnetic-field-induced heating, and substantial cellular internalization. Moreover, the enhanced toxicity to tumor cells by DOX-loaded PMNCs (DOX-PMNCs) under an AC magntic field suggest their potential for combination therapy involving hyperthermia and chemotherapy.

1. Introduction

Magnetic nanoparticles (MNPs) have been a subject of great interest in recent years due to their potential biomedical applications such as carriers for drug delivery, magnetic thermotherapy of cancer cells (hyperthermia), as a contrast agent for magnetic resonance imaging (MRI), and separation of proteins and cells.[1–6] Among MNPs, superparamagnetic magnetite (Fe_3O_4) has been particularly attractive due to its unique magnetic properties and biocompatibility. Iron and its oxides are metabolized and transported through human tissues by proteins such as ferritin, transferritin etc. and thus naturally integrated into tissue physiology. Moreover, these nanoparticles have the advantage of integrating several functionalities in a single structure so as to perform multiple therapeutic and diagnostic functions. For example, MNPs and drug molecules can be co-encapsulated in liposomes/polymeric micelles to perform imaging, magnetic targeting and hyperthermia.[7–9] Such combination therapies are particularly attempted in cancer treatments. Hyperthermia not only increases the concentration of drug carrier at the tumor site by increasing flow and vessel permeability but also enhances the drug toxicity in certain cancer cells that are otherwise drug resistant.[10,11] Owing to these advantages, the combination of hyperthermia and chemotherapy is evolving as an attractive strategy to optimize cancer therapy, as it often results in synergistic effects.[8,12] Surface functionalized superparamagnetic Fe_3O_4 nanoparticles are ideal materials for such combination therapy.

The above applications require that the magnetic nanocarriers to be water-stable, biocompatible and of narrow size distribution.[2,13–16] Also, there is an immediate concern to achieve selective targeting and release of the drug to the diseased site for the in vivo applications. A number of pH responsive delivery vehicles including micelles, nanogels, mesoporous materials, polymer-drug and MNPs-drug conjugates have been developed for pH triggered release of anticancer agents, by exploiting slightly acidic tumor extracellular environment.[9,17–20] The tumor environment is more acidic than blood and other normal organ tisssue. Recently, Lim et al. demonstrated the pH-triggered release of doxorubicin hydrochloride (DOX) from antibody coated magnetic nanocarriers by modulating the π–π interaction between drug and pyrene moiety present at the nanoparticle surface.[20] This novel nanocarrier offered excellent tumor specific targetting, imaging and simulataneous pH-triggered delivery of the drug at the tumor site. A critical step in developing such stimuli responsive carriers for combination therapy is to engineer the surface of MNPs with suitable surface functionality that have numerous free targeting ligands and pH sensitive moieties. The common strategies used for surface functionalization comprise grafting or coating with organic species, including surfactants, polymers or biomolecules, or coating with an inorganic layer, such as silica.[21–24] Peptides are highly responsive to external pH and

Dr. K. C. Barick, Dr. P. A. Hassan
Chemistry Division
Bhabha Atomic Research Centre
Mumbai 400085, India
E-mail: hassan@barc.gov.in

S. Singh, Prof. D. Bahadur
Department of Metallurgical Engineering and Materials Science
Indian Institute of Technology Bombay
Mumbai 40076, India

N. V. Jadhav, Dr. B. N. Pandey
Radiation Biology and Health Sciences Division
Bhabha Atomic Research Centre
Mumbai 400085, India

DOI: 10.1002/adfm.201201140

offer a wide range of side chain chemistry, thus providing possible applications in tissue engineering, delivery of drugs/biomolecules, MRI, and enrichment of proteins.[25–27] In addition, the cellular uptake of therapeutic agents having low membrane permeability can be enhanced by conjugating them with peptides. Peptide-conjugated carriers can successfully transport drugs/proteins across the membranes of many different cell types, and can also traverse the more demanding blood-brain barrier.[28,29] Attractively, peptide moieties can degrade under in vivo conditions to amino acids and hence, have relatively very low toxicity. Thus, peptide shell cross-linked nanocarriers can act as special kind of synthetic vectors because of their low toxicity, simplicity of use and ease of mass production. In addition, the surface charge, functionality and reactivity of peptide shell cross-linked Fe_3O_4 nanocarrier can be easily altered based on targeting sites to enhance the stability and dispersibility of the nanocarriers. The surface charge of the nanocarriers plays an important role in their fate, both in vitro and in vivo.[30,31]

Here, we report the design and development of pH induced charge-conversional peptide mimic shell cross-linked magnetic nanocarriers (PMNCs) that are amenable for combination of hypethermia and chemotherapy. The PMNCs show good aqueous colloidal stability, high magnetization and good heating ability under external AC magnetic field. The terminal amino acid on the shell of magnetic nanocarriers allows us to create functionalized exteriors with high densities of organic moieties (both amine and carboxyl) for conjugation of drug molecules and biolabelling. Specifically, our nanocarriers showed high drug (DOX) loading capacity, sustained drug release profile and cellular internalization, which makes the fomulation suitable for the targeted drug delivery as well as hyperthermia treatment of cancer.

2. Results and Discussion

PMNCs were grown on glycine functionalized Fe_3O_4 magnetic nanoparticles (GMNPs) by Michael addition/amidation reaction as described in the **Scheme 1**. First, the functionalization of Fe_3O_4 nanoparticles with glycine was carried out in situ during co-precipitation of Fe^{2+} and Fe^{3+} ions in basic medium. FTIR spectroscopic studies of GMNPs indicate that glycine is chemisorbed onto the surface of Fe_3O_4 nanoparticles through carboxylate ions (COO^-) thereby leaving free amine (NH_2) groups on the surface (Figure S1, Supporting Information). These GMNPs were chosen as the core material for further fabrication of peptide mimic shell cross-linked Fe_3O_4 magnetic nanocarriers (PMNCs) due to their good aqueous stability and biocompatibility. PMNCs were prepared by reaction between the free amine group of GMNPs and double bond of methyl methacrylate in the ratio of 1:2. Subsequently, the ester moieties were reacted with ethylenediamine and arginine molecules to achieve the peptide mimic shell cross-linked Fe_3O_4 magnetic nanocarriers with multifunctionality. The organic shell grown on GMNPs by Michael addition/amidation reaction composed of many amide linkages involving two amino acids (glycine and arginine) similar to peptides. Thus, we call it as a peptide mimic system, as it is not same as oligopeptides.

The XRD patterns of GMNPs and PMNCs (Figure S2, Supporting Information) reveal the formation of highly crystalline

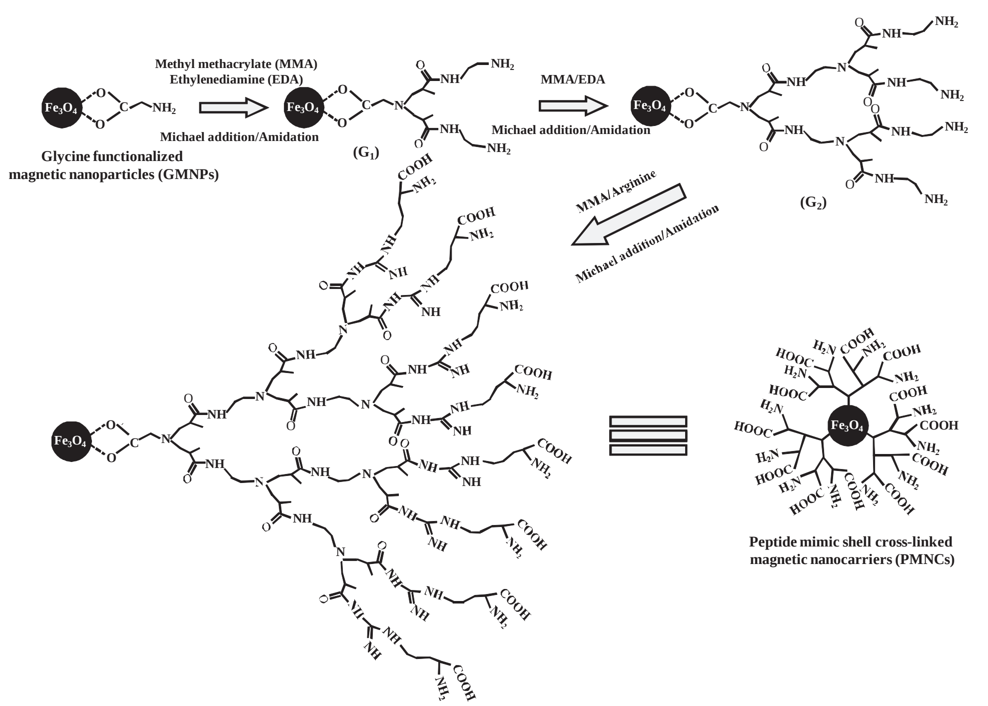

Scheme 1. Schematic representation of the growth of PMNCs for combination therapy.

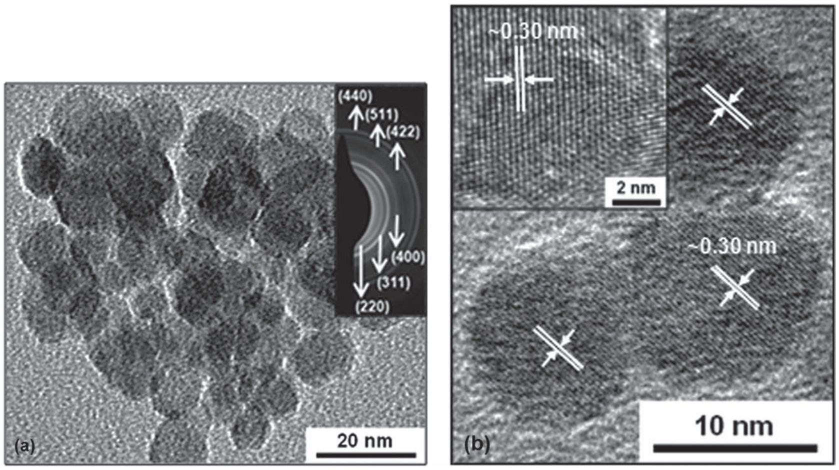

Figure 1. a) TEM image of PMNCs. The inset shows the electron diffraction pattern. b) HRTEM image of PMNCs. The inset shows the high magnification image of the HRTEM.

single phase cubic inverse spinel Fe_3O_4 structure with an average crystallite size of about 10 nm (σ < 10%). The lattice constant was found to be ≈8.378 Å, which is very close to the reported value of magnetite (JCPDS Card No. 88-0315, a = 8.375 Å). From TEM micrographs (**Figure 1**), it is evident that Fe_3O_4 nanoparticles are almost spherical in shape with an average size of ≈10 nm. The electron diffraction pattern (inset of Figure 1a) and HRTEM image (Figure 1b) of PMNCs also confirmed the high crystallinity of their constituents. The electron diffraction pattern can be indexed to (220), (311), (400), (422), (511) and (440) reflections of cubic inverse spinel Fe_3O_4 structure, which is consistent with the XRD results. From HRTEM, the average interfringe distance of Fe_3O_4 nanocarrier was measured to be ≈0.30 nm which corresponds to (220) plane of inverse spinel structured Fe_3O_4.

In order to assess the potential of peptide mimic shell cross-linked nanocarrier in targeted drug delivery and hyperthermia, we have investigated their magnetic properties. These nanocarriers exhibit superparamagnetic behavior without magnetic hysteresis and remanence at 300 K, whereas ferromagnetic behavior with a coercivity of about 235 Oe is observed at 5 K (Figure S3, Supporting Information). This transition from superparamagnetic behavior at room temperature to ferro- or ferrimagnetic behavior below the so-called blocking temperature (T_B = ≈130 K, Figure S4, Supporting Information) is typically observed in MNPs. The maximum magnetizations of PMNCs (at an applied field of 20 kOe) were found to be 50 and 56 emu/g at 300 and 5 K, respectively. The retention of superparamagnetic property at room temperature with biocompatible peptide mimic shell makes these nanocarriers a potential carrier for targeted drug delivery and effective heating source for hyperthermia treatment of cancer cells. Further, the Curie temperature (T_C) of GMNPs and PMNCs were found to be 853 K (Figure S5, Supporting Information) which is in agreement with the reported value for Fe_3O_4 nanoparticles.[15] This suggests that the phase formed is Fe_3O_4 rather than γ-Fe_2O_3, for which the reported Curie temperature is 918 K.[15] The temperature dependant magnetization plot of GMNPs and PMNCs show broad hump in the temperature range of 423–600 K may be assigned to the atomic rearrangement inside the sample or increase in interparticles interaction near the surface because of removal of coated organic moieties at this temperature as indeed suggested from thermogravimetric studies.[2] Further, the broad hump in magnetization versus temperature dependence plot of GMNPs is less prominent as compared to that of PMNCs and absent in case of bare Fe_3O_4 nanoparticles. This further suggests that the broad hump is associated with the removal of organic coating materials.

Now, we look upon the effect of peptide mimic shell cross linking on the structural and interfacial properties of nanocarriers. It can be seen that although most of the FTIR bands from PMNCs correspond well to those of the GMNPs, the FTIR spectra of PMNCs have their own characteristics (Figure S6, Supporting Information). The vibrational modes appeared at 1570 and 1665 cm^{-1} in PMNCs (absent in GMNPs) correspond to the vibration of N-H (2°-amide) II band and C = O (amide I band). The appearance of these additional vibrations in PMNCs suggest the formation of amide linkages during synthesis of peptide mimic shell cross-linked Fe_3O_4 nanocarriers.[32] Further, the presence of ν_s COO^- and ν NH^{3+} bands after coupling with arginine indicates the formation of shell having freely exposed carboxyl and amine groups. Furthermore, FTIR spectra, elemental (CHN) analysis, thermogravimetric studies and magnetic measurements support the formation of organic modification during successive growth of the peptide mimic shell on the surface of GMNPs (Table S1, Figure S6, and Figure S7, Supporting Information). The number of amine groups per particle has been estimated from the nitrogen (N) content in the sample and assuming spherical particles of average diameter 10 nm; the surface density of functional groups were found to be ≈0.95 NH_2/COOH groups per nm^2 (see Supporting Information for details). An increase in the molecular weight of the organic chains attached to the MNPs, during successive growth of the peptide mimic shell, is also manifested from dynamic light scattering (DLS). DLS measurements (Figure S8, Supporting Information) indicate that both GMNPs and PMNCs show monomodal distribution with mean hydrodynamic diameter of 30 and 50 nm, respectvely (polydispersity index ≈ 0.2). The larger hydrodynamic diameter of PMNCs is primarily due to the presence of associated and hydrated long chain organic layers.[2]

A key feature, expected from amino acid functionalities of the PMNCs is negative-to-positive charge conversion upon exposure to an acidic environment. This pH dependent charge-conversional behavior was monitored using zeta-potential (ζ) measurements of the nanocarrier. **Figure 2** shows the variation in the zeta-potential of PMNCs suspension (0.02 mg/ml) at different pH values, as obtained from phase analysis light scattering. From zeta-potential measurements, the pH of zero point charge (pH_{pzc}) of PMNCs was found to be around 5.4. Thus, the PMNCs have net positive surface charge at pH < pH_{pzc} and negative surface charge at pH > pH_{pzc}. This is evident from the changes in the phase difference plots by the application of

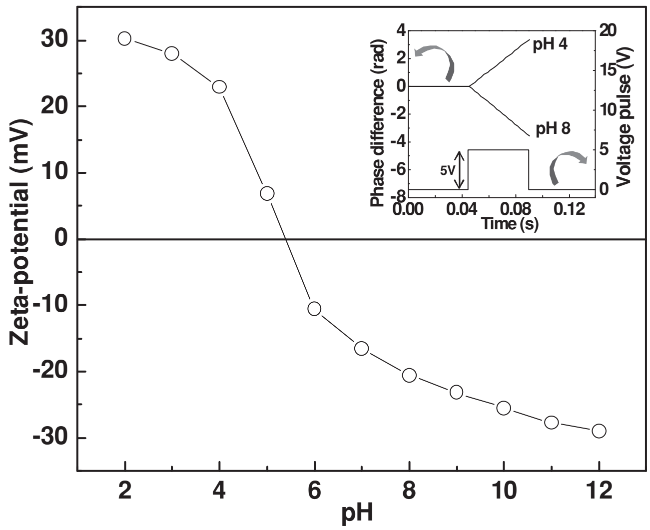

Figure 2. Zeta-potential of 0.02 mg/ml suspension of PMNCs at different pH values. The inset shows the phase difference plot at pH 4 and 8 by the application of voltage pulse.

voltage pulse (field strength = 2.5×10^3 V/m) at two different pH values, 4 and 8 (inset of Figure 2).[33] The reversal of the surface charge of the particles clearly indicates the presence of both NH_2 and COOH groups and it arises from the pH dependant ionization of respective functional groups. A nearly linear variation in the phase difference with time indicates narrow polydispersity of the PMNCs. The dispersibility and colloidal stability of the particles were assessed from the changes in light scattering intensity as well as extinction changes with time. The dispersibility is evident from the increase in absorbance and scattering intensity of the sample when dispersed in aqueous and cell culture media (DMEM + 10% FBS). The insignificant change in absorbance of PMNCs suspensions in aqueous and culture media indicates their good colloidal stability (Figure S9a, Supporting Information). The highly negative values of zeta-potential of these nanocarriers even at low concentration (0.1 mg/ml) in 1% NaCl ($\zeta = -20$ mV) and in 0.01 M PBS, pH 7.3 ($\zeta = -24$ mV) indicate their good colloidal stability in physiological environment. Furthermore, the light scattering intensity and polydispersity index hardly varies with time. The functionalized exteriors (high density of organic spacers, -NH_2 and -COOH) of PMNCs make these particles hydrophilic by formation of hydrogen bonds between surface functional groups and water. In addition, the electrostatic repulsive force originating from the ionization of the surface groups provide additional stability to the particles. The optical images showing PMNCs (0.1 mg/ml) suspended in aqueous and culture media are shown in Figure S9b (Supporting Information). We also addressed the interaction of these nanocarriers with bovine serum albumin (BSA) protein at physiological medium (0.01 M PBS, pH 7.3). The PMNCs do not show any significant change in zeta-potential (Table S2, Supporting Information) and absorbance even after incubation with BSA for 2h, revealing the protein resistance characteristic of PMNCs at physiological medium.

The pH dependant surface charge of peptide functionalized MNPs makes it an attractive vehicle for the delivery of electrostatically bound drug molecules. DOX is chosen as a model cationic drug to estimate the drug loading and release behavior of the PMNCs. DOX is an anthracycline antibiotic which is considered as essential components of first-line chemotherapy in the treatment of a variety of solid and hematopoietic tumors. We employed zeta-potential and fluorescence spectroscopic analysis to investigate the binding of DOX with PMNCs. **Figure 3**a shows the variation in the zeta-potential and Figure 3b shows fluorescence spectra of aqueous suspension of PMNCs and DOX-PMNCs. The zeta-potential of the PMNCs (100 μg/ml suspension) increased from −22.0 mV to −5.0 mV upon incubating with an aqueous solution of 10 μg/ml of DOX. This increase in surface charge arises from the binding of cationic DOX (protonated primary amine present on the drug induces a positive charge) with negatively charged nanocarrier predominately through electrostatic interactions.

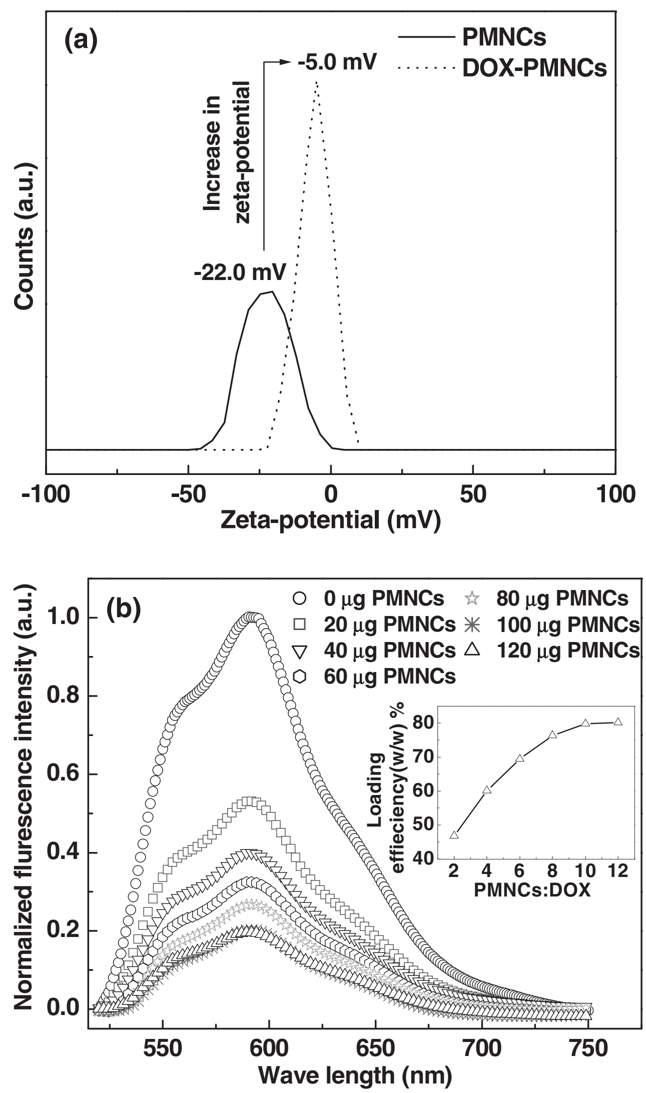

Figure 3. a) Zeta-potential and b) fluorescence spectra of aqueous suspension of PMNCs and DOX-PMNCs. Inset of Figure 3b shows the loading efficiency of DOX onto PMNCs as obtained from the fluorescence measurements.

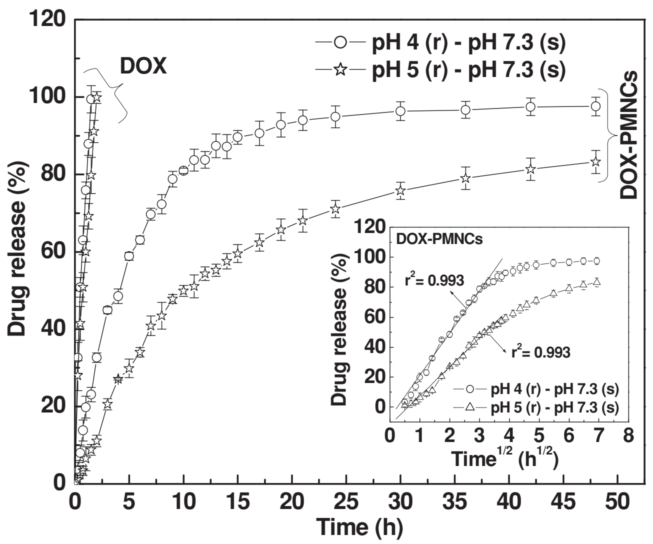

Figure 4. pH dependent drug release profile of pure DOX and DOX-PMNCs in cell mimicking environment (reservoir (r): pH 5/pH 4 and sink (s): pH 7.3) at 37 °C. The inset shows the Higuchi drug release model of DOX-PMNCs.

The affinity of DOX for negatively charged molecules such as citrate ions, oleate ions and phospholipids has been the subject of numerous earlier investigations.[15,34,35] The interaction of DOX molecules with PMNCs was also evident from the decrease in fluorescence intensity of the supernatant liquid after removal of the drug bound PMNCs through magnetic separation. Furthermore, the fluorescence intensity of supernatant liquid decreases with increase in the concentration of PMNCs, which is obvious due to the increase in loading efficiency of DOX onto PMNCs. The efficiency of drug loading onto PMNCs (binding isotherm) was calculated from the concentration of free and bound drug, as obtained from the fluorescence measurements (inset of Figure 3b). It has been observed that loading efficiency is strongly dependent on the ratio of nanocarrier to DOX and a maximum drug loading efficiency (w/w) of about 80% is achieved at PMNCs (in terms of Fe concentration) to DOX ratio of 10 (no significant increase in loading efficiency above this ratio). It is noteworthy to mention that PMNCs still reserve water solubility, good dispersibility, protein resistance characteristics and magnetic response to an external magnetic field after being coupled with DOX molecules.

To mimic the pH dependent drug release profile of pure DOX and DOX-PMNCs in tumor tissue environment, release profiles were investigated under different reservoir-sink conditions (reservoir (r): pH 4/pH 5/pH 7.3 and sink (s): pH 7.3) at a temperature of 37 °C. The physiological pH of blood stream is 7.4, while subcellular lysosomal compartments of tumor cells have pH < 5.0. The drug release studies under reservoir-sink conditions (**Figure 4**) show a strong dependence of the release profile on the reservoir pH values. While pure DOX shows rapid release behavior with $t_{1/2}$ (time needed for the release of 50% of the dose) about 30 min and 45 min at a pH of 4 and 5 respectively, the DOX-PMNCs show sustained release profile at the same pH. The $t_{1/2}$ values observed for DOX-PMNCs are 5 h and 10 h at a pH of 4 and 5, respectively. Furthermore, the short time behavior shows a linear relationship between the drug release and square root of time ($t^{1/2}$) as expected from Higuchi drug release model confirming that the DOX release process is diffusion-controlled (inset of Figure 4).[36] It is interesting to observe from the release profiles that the release rate of DOX is higher at lower pH. This is desirable for cancer therapy as the relatively low pH in tumors will specifically stimulate the DOX release in the target site. The pH triggered release of DOX could be attributed to the weakening of the electrostatic interactions between the drug and the partially neutralized carboxyl groups on the nanoparticle surface, due to a decrease in pH from the zero point charge (PZC). However, the drug release observed in physiological pH (reservoir-sink pH of 7.3) is as little as 7% only, as compared to complete release at pH 4. Our release studies indicate good stability of electrostatically bound drug molecules (DOX-PMNCs system) in physiological pH and triggered release at acidic conditions. Moreover, the action of anticancer drugs like geldanamycin and their analogues based on pH triggered lysosomal targeting of cancer cells has been demonstrated and such approach would be helpful for selective targeting of tumor cells.[37]

The results obtained from drug release studies prompted us to explore the cytotoxicity and cellular uptake of PMNCs on human cancer cell lines since these are critical factors in evaluating the potential of new drug delivery system. The cytotoxicity of PMNCs, pure DOX and DOX-PMNCs was investigated using sulforhodamine B (SRB) assay. Our SRB assay showed that about 90% of the HeLa cells were viable, even after 24 h incubation with 2 mg/ml of PMNCs (Figure S10, Supporting Information). This result suggests that pure nanocarriers do not have toxic effect on HeLa cells. However, DOX and DOX-PMNCs show significant toxicity to the proliferation of HeLa cells (**Figure 5**). Optical microscopic observation suggests that the control cells grow exuberantly, with integrated nucleus

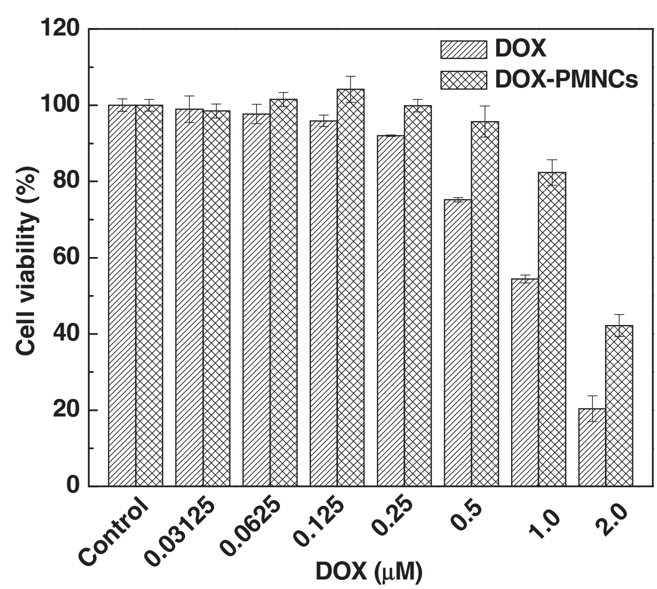

Figure 5. Viabilities of HeLa cells incubated with medium containing DOX and DOX-PMNCs at 37 °C for 48 h.

structure, and distinguishable karyothecas. On the other hand, the cells have undergone morphological changes to nearly spherical shape in the presence of DOX-loaded PMNCs (Figure S11, Supporting Information). The 50% inhibitory concentration (IC_{50}) value for DOX in HeLa cells was found to be 1.08 μM, which is very close to the reported value (1.12 μM).[38] The IC_{50} value of DOX-loaded PMNCs in HeLa cells was estimated to be 1.95 μM (Figure S11, Supporting Information). The relatively higher IC_{50} value (lower cytotoxicity) of DOX-loaded PMNCs, compared to DOX, can be attributed to the sustained release behavior of the nanocarriers (loaded drug is expected to release slowly over the experimental period of 48 h).[18]

The cellular uptake of DOX-PMNCs were monitored by confocal laser scanning microscopy (CLSM). **Figure 6** shows the CLSM images of HeLa cells after incubation with the DOX-PMNCs and lysotracker green at culture conditions. A significant uptake/spatial distribution of DOX-PMNCs were clearly observed from the red fluorescence image arising from DOX emission, suggesting that the drug loaded nanocarriers were internalized in the cells. The green fluorescence image shows emission from lysosomes, stained with lysotracker green. The merged image of DOX and lysotracker fluorescence (as seen by the orange to yellow color) clearly indicates that DOX-PMNCs are partially co-localized in lysosomes. In order to confirm that there is no interference of individual signals from DOX and lysotracker, at the set parameters of CLSM, imaging was also performed for cells treated individually with DOX-PMNCs and lysotracker green (Figure S12, Supporting Information). No fluorescence emission was observed for DOX-PMNCs in the emission window where lysotracker fluorescence is monitored and vice versa. Cellular uptake of DOX-PMNCs was further verified by flow cytometry analysis (**Figure 7**). Compared to control, a distinguishable increase in fluorescence intensity was observed in cells treated with DOX-PMNCs, which was again found to be dependent on DOX-PMNCs concentrations. This indicates significant cellular uptake of DOX-PMNCs. It may also be noted that fluorescence intensity from cells treated with free DOX was found to be higher than that of cells treated with DOX-PMNCs, which is expected as free DOX can readily diffuse in to the cells. The cellular uptake of DOX-PMNCs was also quantified by measuring the iron content per cell using ICP-AES. It has been observed that internalization is dependent on the concentration of carrier and their incubation time. The mean cellular iron content was 8.2 and 65 pg Fe/cell for 1 h for 2 and 8 μM DOX, which was 18.6 and 90 pg Fe/cell after 3 h at these concentrations of DOX, respectively (Figure S14, Supporting Information). This result is in a good agreement with the findings by CLSM and flow cytometry studies. The developed peptide mimic shell cross-linked nanocarriers are seen to behave like amphiphilic cell-penetrating peptides (CCP) which facilitate the cellular transport across the plasma membrane. Our observations of confocal fluorescence microscopy, flow cytometry and SRB assay demonstrate that the use of peptide mimic shell cross-linked nanocarrier as molecular delivery vehicles could significantly enhance the accumulation of drug (DOX) in target cancer cells leading to a high therapeutic efficacy which efficiently inhibit their proliferation.

The combination of hyperthermia and chemotherapy can be employed synergistically for the effective treatmnent of cancer. Site specific heating of the tumor site would improve the efficacy of magnetic thermotherapy. **Figure 8** shows the temperature *vs.* time plot for an aqueous suspension of PMNCs under AC magnetic field (AMF). The results showed a time-dependent gradual increase in temperature. The use of magnetic nanocarriers in thermal therapy depends on their heating efficiency, which is expressed in terms of the specific absorption rate (SAR), as discussed in the experimental section. The SAR of PMNCs (1.2 mg/ml) were determined at different field strengths and were found to be 83.8, 146.7 and 220.1 W/g of

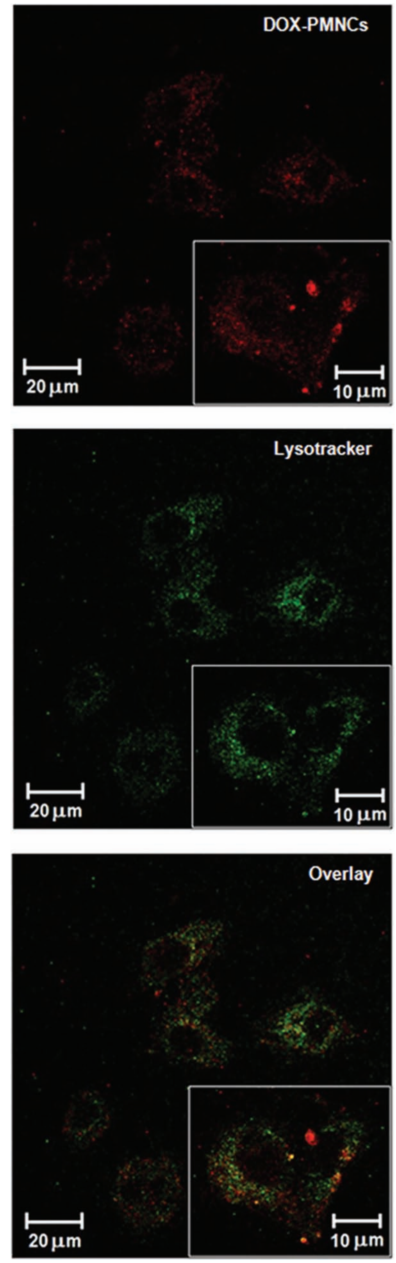

Figure 6. CLSM images of HeLa cells after incubation with the DOX-PMNCs and lysotracker green at culture conditions. The inset shows CLSM images of HeLa cells at higher magnification.

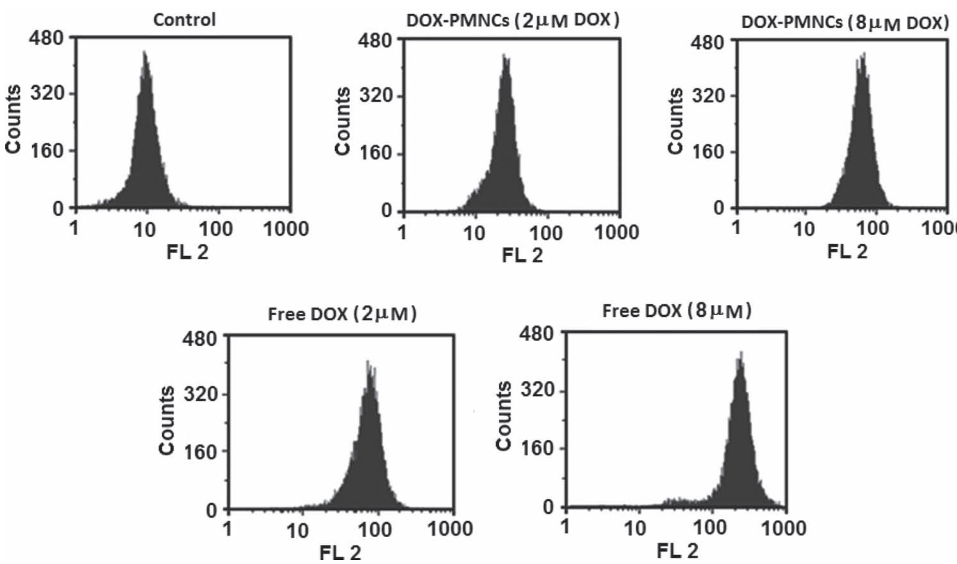

Figure 7. Flow cytometry histograms of HeLa cells treated with DOX-PMNCs and free DOX at culture conditions and at different drug concentrations.

Fe with an applied field of 0.251, 0.335 and 0.419 kOe, respectively (at a fixed frequency of 265 kHz). The observed SAR is likely to be due to a combination of the narrow size distribution of particles and their strong magnetic responsivity (as heating of superparamagnetic nanocarriers in an external AMF is due to Néel and Brownian relaxation loss processes). It has been observed that the time required to reach 43 °C (hyperthermia temperature) decreases with an increase in field strength, which is obvious as the heat generation is proportional to the square of applied AMF (inset of Figure 8). Furthermore, the SAR value of PMNCs (1.2 mg/ml) in cell culture medium (DMEM + 10% FBS) was found to be 132.2 W/g of Fe with an applied field of 335 Oe, which is about 10% less than that observed in aqueous medium (146.7 W/g of Fe). This decrease in SAR value can arise from the blocking of Brownian relaxation contribution as a result of increase in viscosity of the surrounding environment i.e. cell culture medium.[39] In addition to the applied field, SAR is also dependent on magnitude of frequency and physical properties of magnetic particles (magnetization, particles size and size distribution).[21,40]

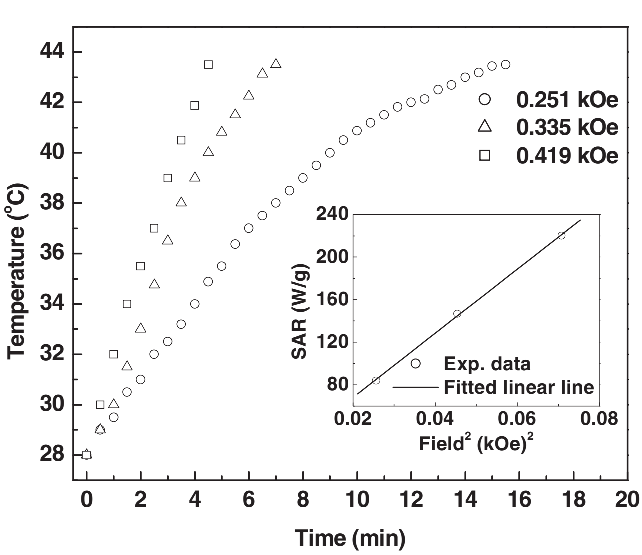

Figure 8. Temperature vs. time plot for an aqueous suspension of PMNCs under AC magnetic field (AMF). The inset shows the linear relationship between SAR and the square of the applied AMF.

We have also addressed the combined effects of magnetic hyperthermia and chemotherapy on HeLa cells (**Figure 9**). Note that the control cells with and without AMF and the PMNCs showed very little decrease (< 3%) in cell viability. However, cells loaded with DOX or DOX-PMNCs showed about 10% decrease in cell viability. It is worth mentioning that PMNCs in the presence of AMF also showed 13% decrease in cell viablity as compared to the marginal decrease in the presence of PMNCs alone. As expected, no further significant decrease in cell viability is observed when DOX loaded cells were subjected to AMF. It is interesting to observe that DOX-PMNCs in combination with AMF (C) showed much higher cytotoxicity (i.e. 28% decrease in cell viability) than individual treatments of PMNCs with AMF (A) and DOX-PMNCs (B). An evaluation using Valeriote's formula showed that the combined effects were synergistic in nature (Table S3, Supporting Information).[41] This study exhibits the potential of peptide mimic shell cross-linked nanocarriers for combination of magnetic hyperthermia and chemotherapy.

3. Conclusions

In summary, we have developed water dispersible, peptide mimic shell cross-linked Fe_3O_4 magnetic nanocarriers of average size about 10 nm with tumor-localized (pH-responsive)

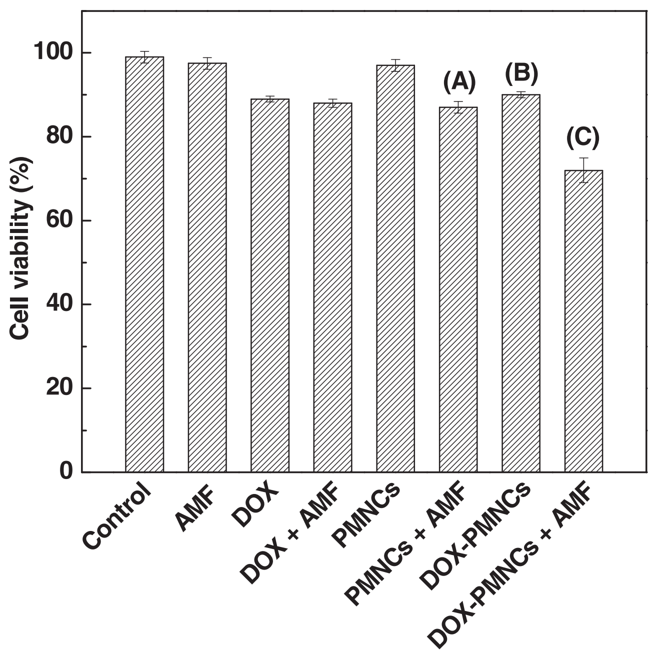

Figure 9. Effect of combination therapy (magnetic hyperthermia and chemotherapy) on HeLa cells using DOX-PMNCs with a DOX concentration of 8 μM along with various control groups.

charge-conversional features for combination of chemotherapy and hyperthermia. These nanocarriers transformed from a negatively charged to a positively charged form in the acidic environment and promoted cargo release, which could remarkably cause cytotoxicity to cancer cells. Furthermore, these peptide mimic shell cross-linked nanocarriers are resistant to protein adsorption under physiological medium. These properties indicate that the creation of magnetic nanocarriers with pH responsive behavior can be applied to design of drug carriers for combining the chemotherapy and hyperthermia. In addition, the multiple functionalities, such as amine and carboxyl groups of the carriers, can be acessed for the conjugation of targeting ligands, such as the folate receptor, for higher intracellular uptake and radiolabeling for magnetically targeted combination therapy involving chemotherapy, hyperthermia, and radiotherapy. Furthermore, the internal cavities of dendritic shell can be also used for entrapment and sustained release of drug molecules.

4. Experimental Section

Materials: Ferrus chloride tetrahydrate ($FeCl_2.4H_2O$, ≥99%), ferric chloride hexahydrate ($FeCl_3.6H_2O$, ACS reagent, 97%), glycine (≥98.5%), bovine serum albumin (BSA, ≥96%), doxorubicin hydrochloride (DOX, >98%), sulforhodamine B (SRB) were procured from Sigma-Aldrich, USA. Methyl methacrylate (99%) was purchased from Merck, Germany. Ethylenediamine (99%), L-arginine monohydrochloride (>99%) and trichloroacetic acid (>99%) were obtained from Spectrochem Pvt. Ltd., India. 25% ammonia solution, methanol and acetic acid (AR grades) were purchased from Thomas Baker Chemical Pvt. Ltd., India. All chemical were used as received.

Synthesis of Glycine Functionalized Magnetic Nanoparticles (GMNPs): In a typical synthesis of glycine functionalized Fe_3O_4 magnetic nanoparticles (GMNPs), $FeCl_3$, $6H_2O$ (5.406 g) and $FeCl_2$, $4H_2O$ (1.988 g) were dissolved in water (80 ml) in a round bottom flask and temperature was slowly increased to 70 °C in refluxing condition under nitrogen atmosphere with constant mechanical stirring at 1000 rpm. The temperature was maintained at 70 °C for 30 min and then 25% ammonia solution (30 ml) was added instantaneously to the reaction mixture, and kept for another 30 min at 70 °C. Then, aqueous solution (4 ml) of glycine (0.3 gm/ml) was added and temperature was slowly raised up to 90 °C under reflux and reacted for 60 min with continuous stirring. The obtained black coloured precipitates were then thoroughly rinsed with water and separated from the supernatant using a permanent magnet.

Synthesis of Peptide Mimic Shell Cross-Linked Fe_3O_4 Magnetic Nanocarriers (PMNCs): Peptide mimic shell cross-linked Fe_3O_4 magnetic nanocarriers (PMNCs) were grown on GMNPs by Michael addition/amidation reaction. In brief, amine terminated GMNPs (1.0 g) were dispersed in methanol (100 ml) containing excess of methyl methacrylate (40 ml). The suspension was ultrasonicated for 10 min and stirred in a rotavapor for 7 h at room temperature. The above treated particles were washed with methanol for 5 times by magnetic separation, then ethylenediamine (12 ml) was added and the suspension was stirred in a rotavapor for another 5 h at 50 °C. Particles were separated by magnetic separation and washed with methanol for 5 times to obtain first generation intermediate (G_1). Above procedure was repeated by successive addition of methyl methacrylate and ethylenediamine to obtain second generation intermediate (G_2). These particles were redispersed in methanol (100 ml) containing methyl methacrylate (40 ml) and stirred in a rotavapor for 7 h at room temperature. Then, particles were thoroughly washed and treated with aqueous solution (40 ml) of L-arginine monohydrochloride (4 gm) at 50 °C for 5 h in a rotavapor to obtain multifunctional (amine and carboxyl terminated) peptide mimic shell cross-linked magnetic nanocarriers.

Characterization: X-ray diffraction (XRD) pattern was recorded on a Philips powder diffractometer PW3040/60 with Cu Kα radiation. The crystallite sizes are estimated from the X-ray line broadening using Scherrer formula. The infrared spectra were recorded in the range 4000–400 cm^{-1} on a Fourier transform infrared spectrometer (FTIR, Magna 550, Nicolet Instruments Corp., USA). The transmission electron micrographs were taken by FEG TEM (JEOL JEM-2100F) for particle size determination. The thermogravimetric analysis (TGA, Model Q50, V6.1 series, TA Instruments, USA) was performed under N_2 atmosphere from room temperature to 550 °C with a heating rate of 10 °C/min. The elemental analysis was carried out by FLASH EA 1112 series CHNS (O) analyzer (Thermo Fennigan, Italy). Dynamic light scattering (DLS) measurements were performed using a Malvern 4800 Autosizer employing a 7132 digital correlator for the determination of hydrodynamic diameter. The zeta-potential measurements were determined by Zetasizer nano series, Malvern Instruments. The stability assay was investigated by measuring the absorbance at wavelength of 350 nm for different time interval at room temperature using JASCO V-650, UV-visible spectrophotometer. The field dependent magnetization and zero field cooled-field cooled (ZFC-FC) measurements at applied field of 100 Oe were carried out by physical property measurement system (PPMS, Quantum Design). The Curie temperature was measured in an applied field of 100 Oe using vibrating sample magnetometer (VSM-7410, LakeShore) under N_2 atmosphere. In order to evaluate the specific absorption rate and cytocompatibility, amount of Fe in suspension of PMNCs was obtained by ICP-AES analysis (Spectro Arcos, German).

Drug Loading and Release: The anticancer agent, doxorubicin hydrochloride (DOX) was used as a model drug to estimate the drug loading and release behavior of the PMNCs. In order to investigate the interaction of drug molecules with PMNCs, we have studied the fluorescence spectra of pure DOX and DOX-PMNCs in addition to zeta-potential measurements. The aqueous dispersion of different amounts of PMNCs (0, 20, 40, 60, 80 and 100 μg from a stock suspension of 2 mg/ml of Fe) were added to a 1 ml of DOX solution (10 μg/ml) and mixed thoroughly by shaking at room temperature for 15 min.

The fluorescence spectra of the supernatant (obtained after magnetic sedimentation of drug loaded PMNCs) were then recorded using Hitachi F 2500 fluorescence spectrophotometer. The fluorescence intensities of supernatants (washed drug molecules were also taken into consideration for calculations) against that of pure DOX solution were used to determine the loading efficiency (binding isotherm of DOX with PMNCs). The loading efficiency (w/w%) was calculated using the following relation:

$$\%\ \text{Loading efficiency} = \frac{I_{DOX} - I_S - I_w}{I_{DOX}} \times 100$$

where, I_{DOX} is the fluorescence intensity of pure DOX solution, I_S the fluorescence intensity of supernatant and I_W the fluorescence intensity of washed DOX (physically adsorbed DOX molecules).

For release study, we have quantified the amount of DOX-PMNCs according to the binding isotherm. The loading was carried out, at increased scale, by incubating 0.5 ml of aqueous solution of DOX (1 mg/ml) with 1 ml of the aqueous suspension (pH ≈ 7.5) of PMNCs (5 mg/ml) for 1 h in dark (however, no decrease in fluorescence intensities was observed after 15 min of incubation). Drug loaded samples were separated from the free-standing drug molecules through magnetic separation and carefully washed by milli Q water. The pH-triggered drug release studies were carried out under reservoir (r) - sink (s) conditions. The drug-loaded PMNCs (5 mg) were immersed into 5 ml of respective release medium (acetate buffer-pH 4, acetate buffer-pH 5 or phosphate buffered saline-pH 7.3) and then put into a dialysis bag. The dialysis was performed against 200 ml of phosphate buffered saline (PBS-pH 7.3) under continuous stirring at 37 °C to mimic the cellular environment. 1 ml of the external medium was withdrawn and replaced with fresh PBS at fixed interval of times to maintain the sink conditions. The amount of doxorubicin released was determined by measuring the fluorescence intensity at $\lambda_{excitation}$ = 490 nm and $\lambda_{emission}$ = 535 ± 35 nm using Perkin Elmer 1420 multilabel counter against the standard plot prepared under similar condition. Each experiment was performed in triplicates and standard deviation was given in the plot. The release data were fitted to the Higuchi model. Higuchi model describes drug release as a diffusion process based on Fick's law according to the equation:

$$Q = k_H t^{1/2}$$

where Q is the amount of drug released at time t, and k_H the Higuchi dissolution constant.

Cell Lines and Culture: Human cervical cancer cell line HeLa was obtained from National Centre for Cell Sciences, Pune, India. Cells were cultured in Dulbaco's Minimal Essesntial Medium (DMEM) supplemented with 10% fetal bovine serum (FBS; Hi-Media, Mumbai, India) and antibiotics (penicillin: 100 Units/ml, streptomycin: 250 μg/ml) in humidified incubator at 5% CO_2 and 37 °C. Wherever required during culture experiemnts, PMNCs loaded with DOX were diluted with same culture medium followed by water bath sonication.

Time-Dependent Calorimetric Measurements (Hyperthermia Studies): The heating ability of sample suspensions was obtained from the time-dependent calorimetric measurements using an induction heating unit. 1 ml (1.2 mg/ml of Fe) of PMNCs suspension was taken in a polypropylene sample holder with suitable arrangements to minimize the heat loss. The AC magnetic field (AMF) of 0.251, 0.335 and 0.419 kOe, and fixed frequency of 265 kHz were used to evaluate the specific absorption rate (SAR). The SAR was calculated using the following equation:

$$SAR = C\frac{\Delta T}{\Delta T}\frac{1}{m_{Fe}}$$

where, C is the specific heat of solvent ($C = C_{water}$ = 4.18 J/g °C), $\Delta T/\Delta t$ is the initial slope of the time-dependent temperature curve and m_{Fe} is mass fraction of Fe in the sample.

Cytotoxicity Studies: Sulforhodamine B (SRB) assay was performed to evaluate cytotoxicity of the PMNCs to HeLa cell lines without induction heating. The cells were seeded into 96-well plates at densities of 1×10^4 cells per well for 24 h. Then different concentrations of PMNCs loaded with DOX (0.03125-2.0 μM DOX) were added to cells and incubated for 48 h at 37 °C and 5% CO_2. Thereafter, the cells were washed thrice with phosphate buffer saline (PBS) and processed for SRB assay to determine the cell viability. For this, cells were fixed with a solution of 50% trichloroacetic acid and stained with 0.4% SRB dissolved in 1% acetic acid. Cell-bound dye was extracted with 10 mM unbuffered Tris buffer solution (pH 10.5) and then absorbance was measured at 560 nm using a plate reader. The cell viability was calculated using the following formula:

$$\%\ \text{Viability} = (\text{Absorbance of treated sample/Absorbance of control}) \times 100$$

In order to prove the potential of the carrier for therapeutic applications, we have evaluated the 50% inhibitory concentration (IC_{50}) values by SRB assay. IC_{50} is defined as the concentration of material that results in a 50% inhibition of cellular processes. For this, HeLa cells were treated with DOX and DOX-PMNCs at different doses. Different dilutions were prepared in culture medium using stock solutions of 4 μM pure DOX and DOX-PMNCs having 4 μM of DOX (to provide an equivalent amount of drug used) in milli Q water. Media from wells were replaced with the above solutions prepared in culture medium. Cells were incubated for another 48 h to determine the cell viability using the SRB assay. The IC_{50} values were calculated using the sigmoidal dose-response equation from Origin 8 software (Origin Lab Corporation, Northampton, MA).

Furthermore, the effect of PMNCs loaded without or with DOX (8 μM) on HeLa cells, which were subjected to induction heating with respective controls, was investigated. Cells (0.5×10^6) were seeded overnight in petridishes (P-60) containing culture medium (4 ml) followed by treatment with PMNCs loaded without or with DOX for 3 h at culture conditions. Subsequently, cells were washed three times with PBS to remove non-internalized particles. Cultures replaced with fresh culture media (4 ml) were subjected to AMF (335 Oe, 10 min.) under sterile conditions using induction heating system as reported earlier.[40] After AMF exposure, cells were further cultured for 2 h and harvested by trypsinization. Cell viability was performed using trypan blue dye exclusion method. Cells treated with different conditions were named as follows: (i) untreated cells (Control), (ii) magnetic field only (AMF), (iii) particles only (PMNCs), (iv) particles followed by AMF (PMNCs + AMF), (v) DOX only (DOX), (vi) DOX followed by AMF (DOX + AMF), (vii) DOX loaded particles only (DOX-PMNCs), and (viii) DOX loaded particles followed by AMF (DOX-PMNCs + AMF).

Cellular Uptakes Studies: Cellular uptake of DOX loaded particles was quantified by ICP-AES analyses, which was further confirmed by flow cytometry and confocal microscopy. For ICP-AES, HeLa cells (0.5×10^6) were seeded overnight followed by treatment with 2 and 8 μM DOX loaded particles for 1 and 3.5 h at culture conditions. Cells were washed with PBS followed by harvesting of cells by trypsinization. An aliquot (10 ml from 1 ml cell suspension) was used to count the cell number and rests of cells were centrifuged to obtain the pellet. The centrifuged cell pellets were disolved in 37% HCl at 70 °C for 1 h. The ICP-AES samples were diluted to a volume of 10 ml for analysis. For flow cytometry analysis, cells (1×10^6) were seeded for overnight in P-100 dishes containing culture medium (10 ml). Cells were treated with 2 and 8 μM DOX loaded particles as well as free DOX (2 and 8 μM) for 3 h in culture conditions followed by washing with PBS and harvesting the cells by trypsinization. The cells were resuspended in culture medium and flow cytometry analysis (*CyFlow Space,* Partec, Germany) was carried out at FL-2 channel (585 nm band-pass filter) for 20,000 cells. Results were analyzed using FloMax software (version 2.0). For confocal microscopy imaging, cells (0.5×10^6) were seeded on glass coverslips and cultured overnight. The cells were then treated with DOX-PMNCs (8 μM DOX) for 3hrs at culture conditions, followed by washing with PBS. The cells were fixed with 2% paraformaldehyde at 4 °C for 30 mins. For lysotracker labelling, fixed cells were treated with 2 μM lysotracker green (Molecular Probes, USA) for 10 min at culture conditions. Cells treated intividually with DOX-PMNCs and lysotracker as well as both were imaged using

FULL PAPER

confocal microscope (LS510 Meta, Carl Ziess, Germany). The excitation source used was an Ar ion laser (488 nm) and emission window was set at 505–525 nm and 575–615 nm for lysotracker and DOX, respectively.

Supporting Information

Supporting Information is available from the Wiley Online Library or from the author.

Acknowledgements

S.S. and N.V.J. contributed equally to this work. The authors thank Dr. R. S. Ningthoujam for facilitating the use of induction heater. The authors also thank Mr. Manjoor Ali and Mrs. R. Vasumathy for CLSM studies and Mr. Prayag Amin for flow cytometry analysis.

Received: April 24, 2012
Published online: July 3, 2012

[1] J. Cheon, J.-H. Lee, *Acc. Chem. Res.* **2008**, *41*, 1630.
[2] K. C. Barick, M. Aslam, Y.-P. Lin, D. Bahadur, P. V. Prasad, V. P. Dravid, *J. Mater. Chem.* **2009**, *19*, 7023.
[3] H. Gu, K. Xu, C. Xu, B. Xu, *Chem. Commun.* **2006**, 941.
[4] S. H. Wang, X. Shi, M. V. Antwerp, Z. Cao, S. D. Swanson, X. Bi, J. R. Baker, *Adv. Funct. Mater.* **2007**, *17*, 3043.
[5] F. Hu, L. Wei, Z. Zhou, Y. Ran, Z. Li, M. Gao, *Adv. Mater.* **2006**, *18*, 2553.
[6] S. Mornet, S. Vasseur, F. Grasset, E. Duguet, *J. Mater. Chem.* **2004**, *14*, 2161.
[7] L. A. Tai, P. J. Tsai, Y. C. Wang, Y. J. Wang, L. W. Lo, C. S. Yang, *Nanotechnology* **2009**, *20*, 135101.
[8] P. Pradhan, J. Giri, F. Rieken, C. Koch, O. Mykhaylyk, M. Döblinger, R. Banerjee, D. Bahadur, C. Plank, *J. Controlled Release* **2010**, *142*, 108.
[9] N. Nasongkla, E. Bey, J. Ren, H. Ai, C. Khemtong, J. S. Guthi, S.-F. Chin, A. D. Sherry, D. A. Boothman, J. Gao, *Nano Lett.* **2006**, *6*, 2427.
[10] G. Kong, M. W. Dewhirst, *Int. J. Hyperthermia* **1999**, *15*, 345.
[11] T. S. Herman, *Cancer Res.* **1983**, *43*, 517.
[12] Y. Itoh, Y. Yamada, Y. Kazaoka, T. Ishiguchi, N. Honda, *Exp. Therapeutic Med.* **2010**, *1*, 319.
[13] K. Cheng, S. Peng, C. Xu, S. Sun, *J. Am. Chem. Soc.* **2009**, *131*, 10637.
[14] Y. M. Huh, Y. W. Jun, H. T. Song, S. Kim, J. S. Choi, J. H. Lee, S. Yoon, K. S. Kim, J. S. Shin, J. S. Suh, J. Cheon, *J. Am. Chem. Soc.* **2005**, *127*, 12387.
[15] S. Nigam, K. C. Barick, D. Bahadur, *J. Magn. Magn. Mater.* **2011**, *323*, 237.
[16] D. Gao, H. Xu, M. A. Philbert, R. Kopelman, *Nano Lett.* **2008**, *8*, 3320.
[17] S. Chandra, S. Mehta, S. Nigam, D. Bahadur, *New J. Chem.* **2010**, *34*, 648.
[18] K. C. Barick, S. Nigam, D. Bahadur, *J. Mater. Chem.* **2010**, *20*, 6446.
[19] Z. Zhou, Y. Shen, J. Tang, M. Fan, E. V. Kirk, W. J. Murdoch, M. Radosz, *Adv. Funct. Mater.* **2009**, *19*, 3580.
[20] E. -K. Lim, Y. -M. Huh, J. Yang, K. Lee, J.-S. Suh, S. Haam, *Adv. Mater.* **2011**, *23*, 2436.
[21] B. Samanta, H. Yan, N. O. Fischer, J. Shi, D. J. Jerry, V. M. Rotello, *J. Mater. Chem.* **2008**, *18*, 1204.
[22] D. Yang, J. Hu, S. Fu, *J. Phys. Chem. C* **2009**, *113*, 7646.
[23] H. H. P. Yiu, H.-J. Niu, E. Biermans, G. Tendeloo, M. J. Rosseinsky, *Adv. Funct. Mater.* **2010**, *20*, 1599.
[24] S. Laurent, D. Forge, M. Port, A. Roch, C. Robic, L. V. Elst, R. N. Muller, *Chem. Rev.* **2008**, *108*, 2064.
[25] M. S. Standley, D. J. Toft, H. Cheng, S. Soukasene, J. Chen, S. M. Raja, V. Band, H. Band, V. L. Cryns, S. I. Stupp, *Cancer Res.* **2010**, *70*, 3020.
[26] S. R. Bull, M. O. Guler, R. E. Bras, T. J. Meade, S. I. Stupp, *Nano Lett.* **2005**, *5*, 1.
[27] L. Ruan, H. Zhang, H. Luo, J. Liu, F. Tang, Y.-K. Shi, X. Zhao, *Proc. Natl. Acad. Sci. USA* **2009**, *106*, 5105.
[28] J. Temsamani, P. Vidal, *Drug Discovery Today* **2004**, *9*, 1012.
[29] C. Wu, S. L. Lo, J. Boulaire, M. L. W. Hong, H. M. Beh, D. Z. Y. Leung, S. Wang, *J. Controlled Release* **2008**, *130*, 140.
[30] V. Mailander, K. Landfester, *Biomacromolecules* **2009**, *10*, 2379.
[31] E. C. Cho, J. Xie, P. A. Wurm, Y. Xia, *Nano Lett.* **2009**, *9*, 1080.
[32] B. Pan, F. Gao, H. Gu, *J. Colloid Interface Sci.* **2005**, *284*, 1.
[33] J. F. Miller, K. Schatzel, B. Vincent, *J. Colloid Interface Sci.* **1991**, *143*, 532.
[34] E. Munnier, F. Tewes, S. Cohen-Jonathan, C. Linassier, L. Douziech-Eyrolles, H. Marchais, M. Soucé, K. Hervé, P. Dubois, I. Chourpa, *Chem. Pharm. Bull.* **2007**, *55*, 1006.
[35] F. A. D. Wolf, K. Nicolay, B. D. Kruijff, *Biochemistry* **1992**, *31*, 9252.
[36] T. J. Higuchi, *J. Pharm. Sci.* **1963**, *52*, 1145.
[37] R. A. Ndolo, D. T. Jacobs, M. L. Forrest, J. P. Krise, *Mol. Cell Pharmacol.* **2010**, *2*, 131.
[38] D. Y. Lu, M. Huang, C. H. Xu, W. Y. Yang, C. X. Hu, L. P. Lin, L. J. Tong, M. H. Li, W. Lu, X. W. Zhang, J. Ding, *BMC Pharmacol.* **2005**, *5*, 11.
[39] A. Tomitaka, T. Koshi, S. Hatsugai,T. Yamada, Y. Takemura, *J. Magn. Magn. Mater.* **2011**, *323*, 1398.
[40] R. Ghosh, L. Pradhan, Y. P. Devi, S. S. Meena, R. Tewari, A. Kumar, S. Sharma, N. S. Gajbhiye, R. K. Vatsa, B. N. Pandey, R. S. Ningthoujam, *J. Mater. Chem.* **2011**, *21*, 13388.
[41] F. Valeriote, H. Lin, *Cancer Chemother. Rep.* **1975**, *59*, 895.